Nanoscale

Accepted Manuscript

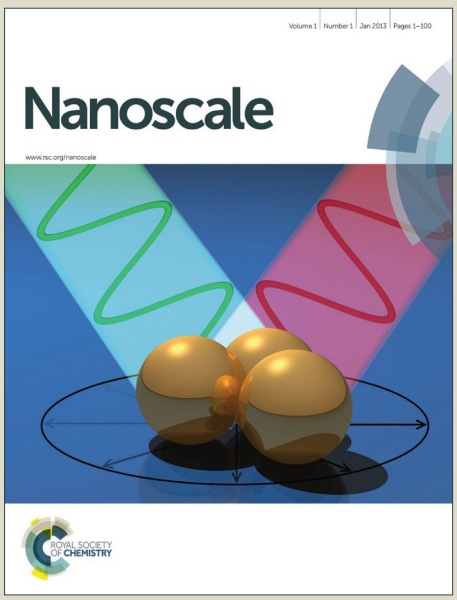

ROYAL SOCIETY OF CHEMISTRY

www.rsc.org/nanoscale

TiO_2 quantum dots as superb compact block layer for high-performance $CH_3NH_3PbI_3$ perovskite solar cells with efficiency of 16.97%

Yongguang Tu, Jihuai Wu*, Min Zheng, Jinghao Huo, Pei Zhou, Zhang Lan, Jianming Lin, Miaoliang Huang

Engineering Research Center of Environment-Friendly Functional Materials for Ministry of Education, Institute of Materials Physical Chemistry, Huaqiao University, Xiamen 361021, China

Abstract: A compact TiO_2 layer is crucial to achieve high-efficiency perovskite solar cells. In this study, we developed a facile, low-cost and efficient method to fabricate a pinhole-free and ultrathin blocking layer based on high crystallized TiO_2 quantum dots (QDs) with an average diameter of 3.6 nm. Surface morphology of the blocking layer and photoelectric performance of the perovskite solar cells were investigated by spin-coating three different materials: colloidal TiO_2 QDs, titanium precursor solution, and aqueous $TiCl_4$. Among these three kinds of treatment, the perovskite solar cell based on TiO_2 QD compact layer offered the highest power conversion efficiency (PCE) of 16.97% with a photocurrent density of 22.48 $mA \cdot cm^{-2}$, photovoltage of 1.063 V and fill factor of 0.71, while the enhancement of PCE mainly stems from small series resistance and large shunt resistance of TiO_2 QD layer.

Key words: perovskite solar cells, TiO_2 quantum dots, compact layer, high crystallinity.

* Corresponding author. Tel: +86-595-22693899; Fax: +86-595-22692229; E-mail address: jhwu@hqu.edu.cn (J. Wu).

1 Introduction

Recently, perovskite organic lead halides (e.g. $CH_3NH_3PbX_3$(X = I, Br, Cl)) have aroused widely interests due to its application in thin film solar cells for making transformative changes.[1-7] The most-studied perovskite light absorbers are $CH_3NH_3PbI_3$[8] and $CH_3NH_3PbI_{3-x}Cl_x$.[9] The superb photovoltaic performances stem from their high light absorption, the long-range charge-transporting property and the low exciton binding energy.[10] $CH_3NH_3PbI_3$ and $CH_3NH_3PbI_{3-x}Cl_x$ are capable of transporting electrons and holes, where the diffusion length is about 130 nm for electrons and about 100 nm for holes in $CH_3NH_3PbI_3$, and ca. 1069 nm for electrons and 1213 nm for holes in $CH_3NH_3PbI_{3-x}Cl_x$.[11,12] Perovskite solar cells are generally composed of transparent conducting oxide substrate (TCO), a n-type compact blocking layer, perovskite layer with or without scaffold layer (e.g. TiO_2, ZnO or Al_2O_3), a p-type hole-transporting material (HTM) layer and metal back electrode. Meanwhile, it is widely recognized that the properties of blocking TiO_2 layer is important.[13] An ideal blocking TiO_2 layer is expected to be ultrathin and pinhole-free. In general, the role of the blocking layer is to prevent direct electrical contact between the TCO and the hole transporting material (HTM), thus reducing charge recombination at this interface.[14-16]

Currently, the n-type compact blocking layer is usually composed of TiO_2, which is mainly fabricated on transparent conducting oxide substrate by spin-coating, spray pyrolysis and atomic layer deposition (ALD) using a titanium precursor solution. For instance, spray pyrolysis was introduced in 1995 by Kavan and Gratzel,[17] and now it is popular in perovskite solar cells as spin-coating method. Also, Wu et al. [18] reported a uniform compact TiO_2 layer with large shunt resistance *(R_{sh})* by ALD and showed superior performance. However, ALD need sophisticated facilities, complicated operations and cost highly. Although simple, spray pyrolysis and spin-coating usually use a titanium precursor solution. Kim[19] has proved that the compact layer prepared by conventional titanium precursor solution possess many

residual organics and hydroxyl groups proved by Fourier transform infrared (FT-IR) and X-ray photoelectron (XPS) spectra. Residual organics and hydroxyl groups are considered as defect of charge collection properties. Hence, a facile, low-cost and efficient approach to fabricate superb compact TiO_2 blocking layer for the perovskite solar cells is imperative.

Herein, the facility of spin-coating approach and high crystallized TiO_2 quantum dots (QDs) were successfully combined together to fabricate a pinhole-free and ultrathin compact blocking layer in the perovskite solar cells. Redispersible colloidal TiO_2 quantum dots (QDs) with an average diameter of 3.6 nm and high crystallinity were successfully synthesized by solvothermal reaction. It has been demonstrated that QD materials such as PbS, CdS, and CdSe QDs can achieve pinhole-free and thickness-controllable compact layer using spin-coating approach.[20,21] Furthermore, surface morphology of the blocking layer and performance of the perovskite solar cells were investigated by spin-coating three different materials: colloidal TiO_2 quantum dots (QDs), titanium precursor solution, aqueous $TiCl_4$. The $CH_3NH_3PbI_3$ perovskite was formed on a mesoporous TiO_2 film using a two-step spin-coating method.[22] Fig. 1 is schematic diagram of the perovskite cell.

2 Experimental

2.1 Materials

All of the materials were purchased from the Sigma-Aldrich Corp., if not specified. The Spiro-OMeTAD was from Materwin New Material Co. Ltd (Shanghai, China).

2.2 Preparation of colloidal TiO_2 quantum dots (QDs)

The TiO_2 QDs with an average diameter of (3.6 ± 0.4 nm) were synthesized by a facile solvothermal reaction reported by Wang et al.[23] and Que et al.[24] In a typical synthesis, 7 mL oleicacid was added into 20 mL hexanaphthene slowly with stirring at room temperatures, followed by adding 5 mL octadecylamine and 1 mL tetra-n-butyl titanate, leading to a yellow

solution. Then the mixture was added to a 50 ml autoclave and reacted at 180 °C for 24 h. After cooled to room temperature, the products was then mixed with 200 mL absolute ethanol and centrifuged to collect the precipitate. Finally, the as obtained product was re-dispersed in 24 mL toluene, obtaining a stable colloidal TiO_2 quantum dot solution.

2.3 Synthesis of CH_3NH_3I

CH_3NH_3I was synthesized according to a reported procedure.[25] CH_3NH_2 (38 ml, 33% in absolute ethanol, Aldrich) and HI (40 ml, 57 wt% in water, Aldrich) were mixed at 0 °C and stirred for 2 h. The precipitate was recovered by evaporation at 50 °C for 1 h. The product was washed with diethyl ether three times and then dried at 60 °C in a vacuum oven for 24 h.

2.4 Preparation of compact TiO_2 blocking layer

Fluorine-doped tin oxide-coated (FTO) glass (Pilkington, TEC-8, 14Ω/sq) was patterned by etching with Zn powder and 2 M HCl diluted solution in deionized water and cleaned by UV-ozone treatment for 15 min, followed by cleaning with detergent and ethanol consecutively. The TiO_2 compact blocking layers were deposited on FTO glass. The first kind of TiO_2 compact layer is based on as-prepared TiO_2 QDs, termed as QD-CL. The second kind of TiO_2 compact layer is based on titanium precursor solution, which was prepared by spin-coating 0.15 M titanium diisopropoxide bis(acetylacetonate) (75 wt% in isopropanol, Aldrich) in 1-butanol (99.8%, Aldrich) solution, termed as TAA-CL. The third kind of TiO_2 compact layer is based on 0.2 M aqueous $TiCl_4$, termed as $TiCl_4$-CL. To probe the effect of compact layer thickness on device performance, each of three different materials was spun at 1000, 2000, 4000, and 6000 rpm for 30 s, respectively. Then they were annealed at 450 °C for 30 min.

2.5 Fabrication of perovskite solar cells

A mesoporous TiO_2 film was deposited on three kinds of TiO_2 compact layer by spin-coating TiO_2 paste diluted in ethanol. TiO_2 paste was prepared as described previously

and the optimal ratio (ethyl cellulose/TiO_2) in the TiO_2 paste was carefully controlled.[26-28] After drying at 100 °C for 5 min, the film was annealed at 450 °C for 30 min, providing a thickness of ~200 nm. The mesoporous TiO_2 film was immersed in 0.02 M aqueous $TiCl_4$ solution at 70 °C for 30 min. After washing with deionized water and alcohol, the film was heated at 500 °C for 30 min. $CH_3NH_3PbI_3$ was formed using two-step spin-coating procedure.[22] PbI_2 solution (1 M) was prepared by dissolving 462 mg PbI_2 (99%, Aldrich) in 1 mL N,N-dimethylformamide (DMF, 99.8%, Aldrich) under stirring at 70 °C. PbI_2 solution (20 μL) was spin-coated on the mesoporous TiO_2 film at 3000 rpm for 5 s and 6000 rpm for 5 s (without loading time). After spinning, the film was dried at 40 °C for 3 min and then 100 °C for 5 min to remove solvent, and after cooling to room temperature, 200 μl of 6.5 $mg \cdot ml^{-1}$ CH_3NH_3I solution in 2-propanol was loaded on the PbI_2-coated substrate for 40 s (loading time), which was spun at 4000 rpm for 20 s and dried at room temperature for 10 min and 100 °C for 5 min. A volume of 20 μL of 2,2',7,7'-tetrakis(N,N-di-p-methoxyphenylamine)-9,9-spirobifluorene (spiro-OMeTAD) solution was spin-coated on the $CH_3NH_3PbI_3$ perovskite layer at 5000 rpm for 30 s. A spiro-OMeTAD solution was prepared by dissolving 72.3 mg of spiro-OMeTAD in 1 mL of chlorobenzene, to which 28.8 μL of 4-tert-butyl pyridine and 17.5 μL of lithium bis(trifluoromethanesulfonyl)imide (Li-TFSI) solution (520 mg LI-TSFI in 1 mL acetonitrile, Sigma-Aldrich, 99.8%) were added. All devices were stored in a desiccator (humidity < 20%) in the dark for 12 h. Finally, 80 nm of gold was deposited under vacuum through a shadow mask.

2.6 Characterization

The crystalline structures of TiO_2 QDs were examined by an X-ray diffraction (XRD, Bruker AXS, D8 Advance). Transmission electron microscopy (TEM) was conducted by a JEOL-2010 TEM. The morphologies of the compact layers and perovskite films were imaged by field-emission scanning electron microscopy (SEM, Hitachi S-4800, Japan). Impedance

spectra (IS) for the solar cell were measured on a ZAHNER IM6e electrochemical workstation under 1 sun AM 1.5 illumination, by applying 0 V DC bias and a 5 mV voltage perturbation in the frequency range 0.1 to 10^5 Hz. The impedance spectra were analyzed with the Zview software. IPCE curves were measured as a function of wavelength from 300 nm to 800 nm using the Newport IPCE system (Newport, USA). The current density-voltage *(J-V)* curves were measured using a Keithley 2401 source-measure unit under AM1.5G illumination at 100 $mW \cdot cm^{-2}$ provided by an Oriel Sol3A solar simulator in ambient environment. The light intensity was adjusted using a NREL-calibrated Si solar cell equipped with KG-2 filter. During the measurement, the photovoltaic devices were masked by a metal aperture to confine the active area (0.125 cm^2).

3 Results and discussion

3.1 Morphology and structure of TiO_2 QDs

Fig. 2 (a) shows the low-magnification TEM image of TiO_2 QDs with an average diameter of (3.6 ± 0.4 nm), as shown in Fig. 2 (b). To analyze the fringe patterns in a TiO_2 QD, we further magnified the TEM image, as shown in Fig. 2 (c). Clearly visible atomic lattice fringes can be seen in Fig. 2 (c), suggesting high crystallinity. Selected area electron diffraction (SAED) pattern is shown in Fig. 2 (d). HRTEM image and SAED patterns reveal that the TiO_2 QDs show polycrystalline phases of anatase TiO_2 with (101) interplanar space of 3.52 Å and (001) interplanar space of 4.84 Å.[29-31] The XRD pattern in Fig. 2 (e) also shows a series of narrow diffraction peaks which correspond to the anatase structure (JCPDS #21-1272) without any other crystalline impurity phases and indicates high crystallinity. Digital photos of colloidal TiO_2 QDs in Fig. 2 (f) reveals a stable and transparent colloid. EDS graph in Fig. 2 (g) and atomic content in Table 1 of TiO_2 QDs show only Ti and O elements in the QDs (C elements stems from carbon film on copper net during TEM test).

3.2 Optimized compact layer

To probe the effect of blocking layer thickness on device performance, each of three different materials was spun at 1000, 2000, 4000, and 6000 rpm for 30 s, respectively. Table 2 shows the device parameters of perovskite solar cells based on $TiCl_4$-CL with different thickness (Cross-sectional SEM image is in Fig. S1). In particular, due to the low saturated vapor pressure and low volatile solvent of water, it is difficult to obtain a uniform layer in low speed, which can be seen from Fig. S1. Table 3 shows the device parameters of perovskite solar cells based on TAA-CL with different thickness (Cross-sectional SEM image is in Fig. S2). Table 4 shows photovoltaic parameters of the perovskite solar cells based on QD-CL with different thickness (Cross-sectional SEM image is in Fig. S3). If a too thick compact layer was applied, the distance of electron from the absorber to FTO will be enlarged, producing more recombination centers. If a too thin compact layer was applied, the FTO will be not fully covered with the dense blocking layer since the surface of FTO substrate is rough because of the F-doped SnO_2 grains with sizes ranging from tens to hundreds of nanometers.[32] Therefore, with decreasing thickness of the TiO_2 compact layer, the performance of solar cells first increased and then decreased. The optimal thickness of three kinds of compact layer is about 50 nm. So we selected 4000 rpm as the optimal spin-coating speed to fabricate compact layer.

Fig. 3 shows the surface morphology of the three compact TiO_2 layers at 4000 rpm for 30 s. Fig. 3 (a) is bare FTO. Fig. 3 (b) ~ (d) are QD-CL, TAA-CL, $TiCl_4$-CL. As is shown in Fig. 3 (a), FTO substrate is rough because of the F-doped SnO_2 grains with sizes ranging from tens to hundreds of nanometers. For the optimized compact layer, the surface morphology of underlying FTO was reserved. For QD-CL sample, highly crystallized TiO_2 QDs with size 3.6 ± 0.4 nm were dispersed in toluene, and easily duplicated the surface morphology of underlying FTO, except for the crevice caused by very large F-doped SnO_2

grains. It can be seen from the inset in Fig. 3 (b) that TiO_2 particles are closely encapsulated on the SnO_2 grains, which can afford a solid blocking effect.

3.3 Photovoltaic performance

J-V measurements of the perovskite solar cells (PSCs) based on three kinds of compact layers at 4000 rpm are shown in Fig. 4 and corresponding photovoltaic parameters are listed in Table 5. The corresponding incident-photon-to-current conversion efficiency (IPCE) spectra of the three devices are shown in Fig. 5. The PSCs with $TiCl_4$-CL, TAA-CL and QD-CL exhibit power conversion efficiency (PCE) of 12.54 %, 14.01 % and 16.97%. To ensure the credibility of the results, a batch of three kinds of perovskite solar cells, containing 27 cells, were prepared and tested under the same conditions, the statistic results are shown in Fig. S4.

Fig. 6 is top-view SEM image of perovskite $CH_3NH_3PbI_3$ film coated on the mesoporous TiO_2 film. The cuboids average size is 700 nm. The larger-sized cuboids can afford a higher J_{SC} due to light scattering and less grain boundaries.[33] From Fig. 4 and Table 5, compared to the PSCs with TAA-CL and $TiCl_4$-CL, the performance improvement for the PSC with TiO_2 QD-CL mainly lies on the increase of FF and V_{OC}.

As is well known, V_{OC} and FF depend largely on the series resistances (R_s) and shunt resistance (R_{sh}) values of the cells.[13, 34, 35] Series resistance (R_s) and shunt resistances (R_{sh}) were estimated using the Keithley 2401 testing system and the results are summarized in Table 5. The R_{sh} values of the PSCs based on QD-CL, TAA-CL, and $TiCl_4$-CL are 6404, 1640, and 955 Ω cm^2, respectively. The R_s values of the PSCs based on QD-CL, TAA-CL, and $TiCl_4$-CL are 5.4, 8.2, and 10.5 Ω cm^2, respectively, which the R_s change order are further confirmed by the electrochemical impedance spectroscopy (EIS, Table S1). Among them, the smallest R_s value for the device based QD-CL stems from both the smaller contact resistance

and the bulk resistance of the QD-CL, which indicates that high photocurrents are anticipated to be generated. It is known that R_{sh} is closely related to the charge recombination at interfaces inside the solar cell. The largest R_{sh} value for the device based QD-CL indicates that short circuits or current leakages are minimized.[36] Higher R_{sh} and lower R_s enable a larger FF and a high electron mobility.[34] These results are in good agreement with the conclusion by analyzing the solar cells performance.

As shown in Fig. 7, we used a simple model capable (equivalent circuit is inset) of producing a good fit to the experimental data.[37] The radius of the impedance semi-circles corresponds to the internal resistances of the $TiO_2/CH_3NH_3PbI_3$ interface, the TiO_2 layer itself and the FTO/TiO_2 interface.[38] The PSC with QD-CL exhibits the lowest ending resistance of the semicircles, indicating the smallest internal resistance among all of the different solar cells (Fitting parameters for EIS data acquired under 1 sun illumination is shown in Table S1). Therefore, the PSC with QD-CL possesses superior charge injection characteristics and low internal resistance. The origin of the different charge collection properties is considered to be due to imperfections such as residual chemicals, hydroxyl groups, and Ti^{3+} ions.[19]

4 Conclusions

In conclusion, a pinhole-free and ultrathin blocking layer based on high crystallized colloidal TiO_2 quantum dots (QDs) with size 3.6 ± 0.4 nm is fabricated successfully by a facile, low-cost and efficient method. The best-performing perovskite solar cell, using a TiO_2 QD compact layer, has achieved a PCE of 16.97% with a high V_{OC} of 1.063 V, a high J_{SC} of 22.48 mA cm^{-2}, and a FF of 0.71, much higher than those of our reference cells using a TAA compact layer and $TiCl_4$ compact layer. The outstanding performance of the perovskite solar cells based on TiO_2 QD compact layer stems from a small series resistance and a large shunt resistance and is confirmed by impedance spectroscopic. This study opens a new direction to

fabricate a pinhole-free and ultrathin blocking layer and push the performance of organic-inorganic lead halide perovskite solar cells to a higher level.

Supporting Information

Table S1. Fitting parameters for EIS data.

Fig. S1 Cross-sectional SEM images of $TiCl_4$-CL with different spin-coating speed.

Fig. S2 Cross-sectional SEM images of TAA-CL with different spin-coating speed.

Fig. S3 Cross-sectional SEM images of QD-CL with different spin-coating speed.

Fig. S4 Photovoltaic parameters of (a) V_{OC}, (b) J_{SC}, (c) FF and (d) PCE extracted from I-V measurements of the solar cells based on QD-CL, TAA-CL, $TiCl_4$-CL (Each parameters is calculated from a batch of 27 cells).

Acknowledgements

The authors acknowledge the financial joint support by the National Natural Science Foundation of China (Nos. 90922028, U1205112, 51472094, 61474047, 21301060, 61306077), the Cultivation Program for Postgraduate in Scientific Research Innovation Ability of Huaqiao University (No. 1400102002).

References

1 A. Kojima, K. Teshima, Y. Shirai and T. Miyasaka, *J. Am. Chem. Soc.*, 2009, **131**, 6050-6051.

2 J. H. Im, C. R. Lee, J. W. Lee, S. W. Park and N. G. Park, *Nanoscale*, 2011, **3**, 4088-4093.

3 H.-S. Kim, C.-R. Lee, J.-H. Im, K.-B. Lee, T. Moehl, A. Marchioro, S.-J. Moon, R.

Humphry-Baker, J.-H. Yum, J. E. Moser, M. Grätzel and N.-G. Park, *Sci. Rep.*, 2012, **2**, 591.

4 M. M. Lee, J. Teuscher, T. Miyasaka, T. N. Murakami and H. J. Snaith, *Science*, 2012, **338**, 643-647.

5 J. Burschka, N. Pellet, S. J. Moon, R. Humphry-Baker, P. Gao, M. K. Nazeeruddin and M. Gratzel, *Nature*, 2013, **499**, 316-319.

6 D. Shi, R. Comin,M. Yuan, E. Alarousu, A. Buin, Y. Chen, S. Hoogland, A. Rothenberger,K. Katsiev, Y. Losovyj, X. Zhang, P.-A. Dowben,O.-F. Mohammed, E.-H. Sargent and O.-M. Bakr, *Science*, 2015,**347**, 519-522.

7 W. Nie, R. Asadpour, J.-C. Blancon, A. -J. Neukirch, G. Gupta, J. -J. Crochet, M. Chhowalla, S. Tretiak, M. -A. Alam, H.-L. Wang and A. -D. Mohite, *Science*, 2015, **347**, 522-525.

8 A. Mei, X. Li, L. Liu, Z. Ku, T. Liu, Y. Rong, M. Xu, M. Hu, J. Chen, Y. Yang, M. Gratzel and H. Han, *Science*, 2014, **345**, 295-298.

9 P. W. Liang, C. Y. Liao, C. C. Chueh, F. Zuo, S. T. Williams, X. K. Xin, J. Lin and A. K. Jen, *Adv. Mater.*, 2014, **26**, 3748-3754.

10 V. D. Innocenzo, G. Grancini, M. J. Alcocer, A. R. Kandada, S. D. Stranks, M. M. Lee, G. Lanzani, H. J. Snaith and A. Petrozza, *Nat. Commun.*, 2014, **5**, 4586.

11 G. Xing, N. Mathews, S. Sun, S. S. Lim, Y. M. Lam, M. Gratzel, S. Mhaisalkar and T. C. Sum, *Science*, 2013, **342**, 344-347.

12 S. D. Stranks, G. E. Eperon, G. Grancini, C. Menelaou, M. J. Alcocer, T. Leijtens, L. M. Herz, A. Petrozza and H. J. Snaith, *Science*, 2013, **342**, 341-344.

13 A. Yella, L. P. Heiniger, P. Gao, M. K. Nazeeruddin and M. Gratzel, *Nano Lett.*, 2014, **14**, 2591-2596.

14 Q. Hu, J. Wu, C. Jiang, T. Liu, X. Que, R. Zhu and Q. Gong, *ACS nano*, 2014, **8**,

10161-10167.

15 L. Kavan, N. Tétreault, T. Moehl and M. Gratzel, *J. Phys. Chem. C*, 2014, **118**, 16408-16418.

16 S. Kazim, M. K. Nazeeruddin, M. Gratzel and S. Ahmad, *Angew. Chem. Int. Ed. Engl.*, 2014, **53**, 2812-2824.

17 M. G. Ladislav Kavan, *Electrochim. Acta*, 1995, **40**, 643-652.

18 Y. Wu, X. Yang, H. Chen, K. Zhang, C. Qin, J. Liu, W. Peng, A. Islam, E. Bi, F. Ye, M. Yin, P. Zhang and L. Han, *Appl. Phys. Express* ,2014, **052301**, 1-4.

19 B. Kim, D. -H. Kim, Y. -Y. Lee,H.-W. Shinc, G. -S. Han, J. -S. Hong, K. Mahmood, T. -K. Ahn, Y. -C. Joo, K. -S. Hong, N.-G. Park, S. Lee and H. -S Jung, *Energy Environ. Sci.*, 2015, **8**, 916-921.

20 A. H. Ip, R. Debnath, I. J. Kramer, S. M. T. , L. L. , Z. N. , A. and E. H. S. , *Nat. Nanotech.*, 2012, **7**, 577-582.

21 J. Gao, C. L. Perkins, J. M. Luther, M. C. Hanna, H. Y. Chen, O. E. Semonin, A. J. Nozik, R. J. Ellingson and M. C. Beard, *Nano Lett.*, 2011, **11**, 3263-3266.

22 J. H. Im, I. H. Jang, N. Pellet, M. Gratzel and N. G. Park, *Nat. Nanotech.*, 2014, **9**, 927-932.

23 X. Wang, J. Zhuang, Q. Peng and Y. Li, *Nature*, 2005, **437**, 121-124.

24 L. Que, Z. Lan, W. Wu, J. Wu, J. Lin and M. Huang, *J. Power Sources*, 2014, **268**, 670-676.

25 Z. Zhu, J. Ma, Z. Wang, C. Mu, Z. Fan, L. Du, Y. Bai, L. Fan, H. Yan, D. L. Phillips and S. Yang, *J. Am. Chem. Soc.*, 2014, **136**, 3760-3763.

26 J. Wu, S. Hao, Z. Lan, J. Lin, M. Huang, Y. Huang, P. Li, S. Yin and T. Sato, *J. Am. Chem. Soc.*, 2008, **130**, 11568-11569.

27 J. H. Wu, Z. Lan, J. M. Lin, M. L. Huang, S. C. Hao, T. Sato and S. Yin, *Adv. Mater.*,

2007, **19**, 4006-4011.

28 J. Lee, D. Seol, A. Cho and N. Park, *Adv. Mater.,* 2014, **26**, 4991-4998..

29 W. Q. Wu, H. S. Rao, Y. F. Xu, Y. F. Wang, C. Y. Su and D. B. Kuang, *Sci. Rep.*, 2013, **3**, 1892.

30 W. Q. Wu, B. X. Lei, H. S. Rao, Y. F. Xu, Y. F. Wang, C. Y. Su and D. B. Kuang, *Sci. Rep.*, 2013, **3**, 1352.

31 G. Tian, K. Pan, Y. Chen, J. Zhou, X. Miao, W. Zhou, R. Wang and H. Fu, *J. Power Sources*, 2013, **238**, 350-355.

32 H. Choi, C. Nahm, J. Kim, J. Moon, S. Nam, D.-R. Jung and B. Park, *Curr. Appl. Phys.*, 2012, **12**, 737-741.

33 Q. Dong, Y. Yuan, Y. Shao, Y. Fang, Q. Wang and J. Huang, *Energy Environ. Sci.*, 2015, **8**, 2464-2470.

34 W. Ke, G. Fang, Q. Liu, L. Xiong, P. Qin, H. Tao, J. Wang, H. Lei, B. Li, J. Wan, G. Yang and Y. Yan, *J. Am. Chem. Soc.*, 2015, **137,** 6730–6733.

35 W. Ke, G. Fang, J. Wan, H. Tao, Q. Liu, L. Xiong, P. Qin, J. Wang, H. Lei, G. Yang, M. Qin, X. Zhao and Y. Yan, *Nat. Commun.*, 2015, **6**, 6700.

36 K. Wang, C. Liu, P. Du, J. Zheng and X. Gong, *Energy Environ. Sci.*, 2015, **8**, 1245-1255.

37 D. Liu, J. Yang and T. L. Kelly, *J. Am. Chem. Soc.*, 2014, **136**, 17116-17122.

38 D.-Y. Son, K.-H. Bae, H.-S. Kim and N.-G. Park, *J. Phys. Chem. C*, 2015, **119**, 10321-10328.

Figure and Table Captions

Fig. 1 Schematic diagram of perovskite solar cell.

Fig. 2 (a) TEM image of TiO_2 QDs, (b) Size distribution histogram of TiO_2 QDs taken from 350 particles, (c) HRTEM image of TiO_2 QDs, (d) SAED image of TiO_2 QDs, (e) XRD of TiO_2 QDs, (f) Digital photos of TiO_2 colloid QDs, (g) EDS graph of TiO_2 QDs.

Fig. 3 Top view SEM images of (a) bare FTO; (b) TiO_2 QD compact layer (inset is HRSEM); (c) TAA compact layer; (d) $TiCl_4$ compact layer.

Fig. 4 J-V curves of the perovskite solar cells based on QD-CL, TAA-CL, and $TiCl_4$-CL.

Fig. 5 IPCE spectra of the perovskite solar cells based on QD-CL, TAA-CL, and $TiCl_4$-CL.

Fig. 6 Top-view SEM image of perovskite $CH_3NH_3PbI_3$ coated on the mesoporous TiO_2 film.

Fig. 7 Nyquist plots of the perovskite solar cells based QD-CL, TAA-CL, $TiCl_4$-CL.

Table 1 Atomic content of TiO_2 QDs

Table 2 Photovoltaic performances of the PSCs based on $TiCl_4$-CL with different spin-coating speed and thickness.

Table 3 Photovoltaic performances of the PSCs based on TAA-CL with different spin-coating speed and thickness.

Table 4 Photovoltaic performances of the PSCs based on QD-CL with different spin-coating speed and thickness.

Table 5 Photovoltaic and resistance parameters of the PSCs with different compact layers.

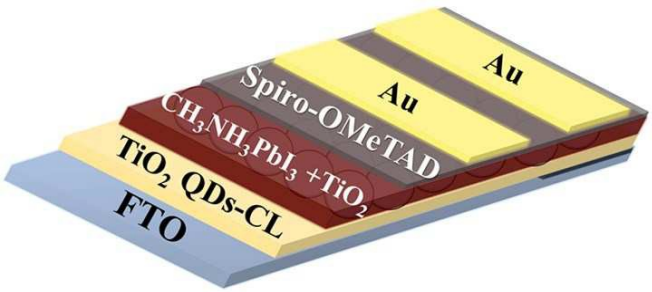

Fig. 1 Schematic diagram of the perovskite solar cell.

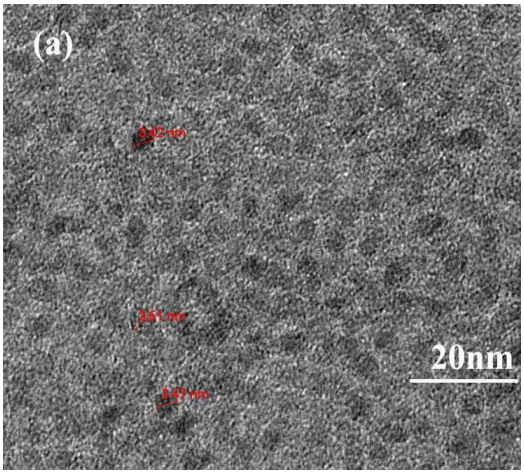

Fig. 2 (a) TEM image of TiO_2 QDs.

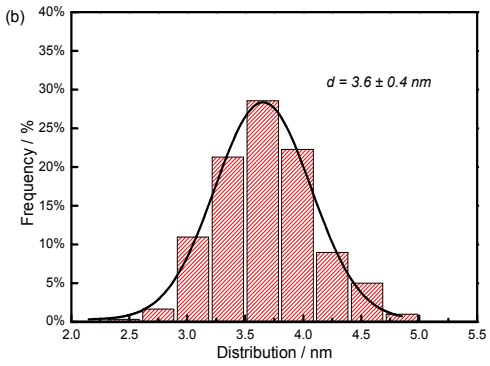

Fig. 2 (b) Size distribution histogram of TiO_2 QDs taken from 350 particles.

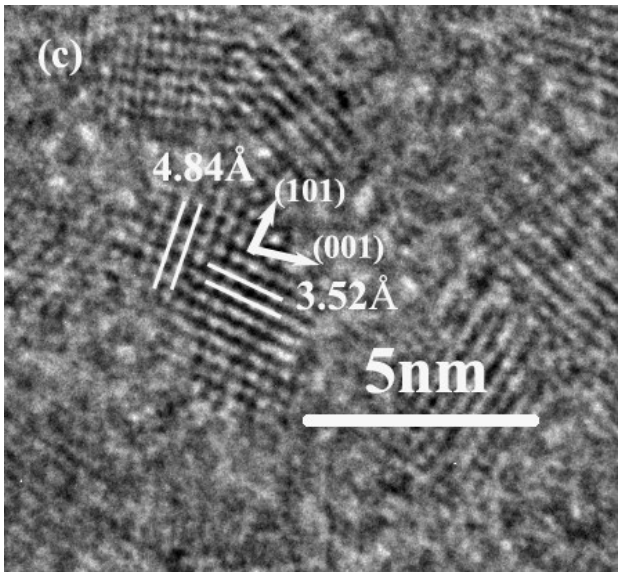

Fig. 2 (c) HRTEM image of TiO_2 QDs.

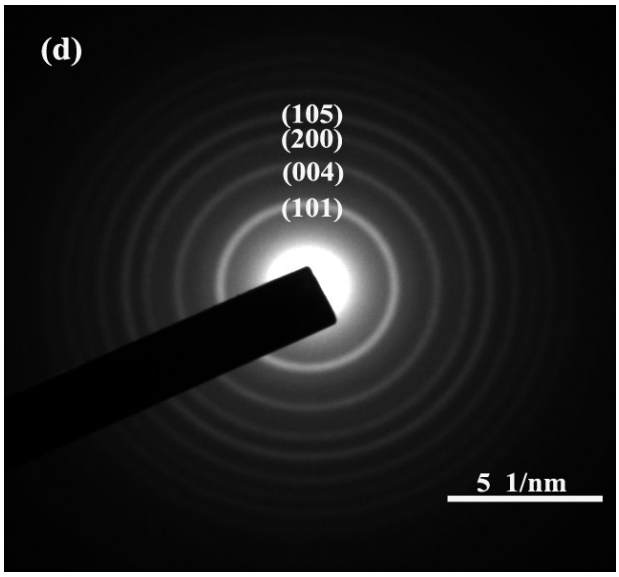

Fig. 2 (d) SAED image of TiO_2 QD.

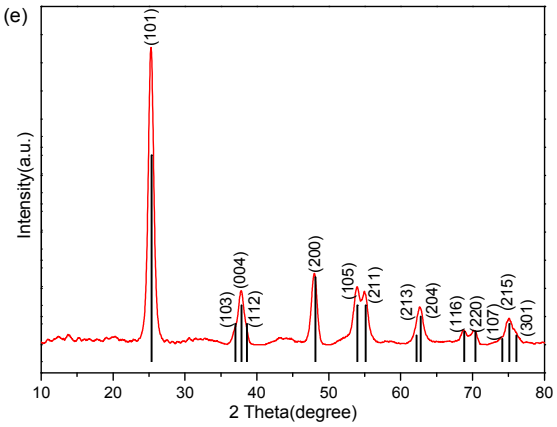

Fig. 2 (e) XRD of TiO_2 QDs.

Fig. 2 (f) Digital photos of TiO_2 colloid QDs.

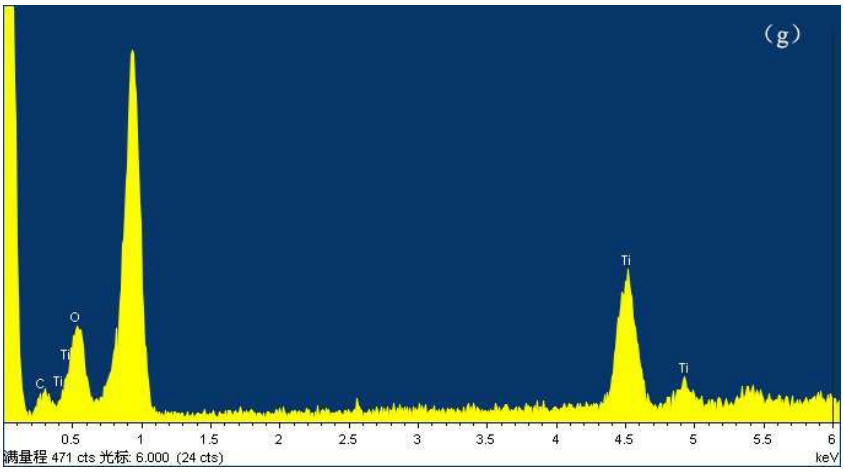

Fig. 2 (g) EDS graph of TiO_2 QDs.

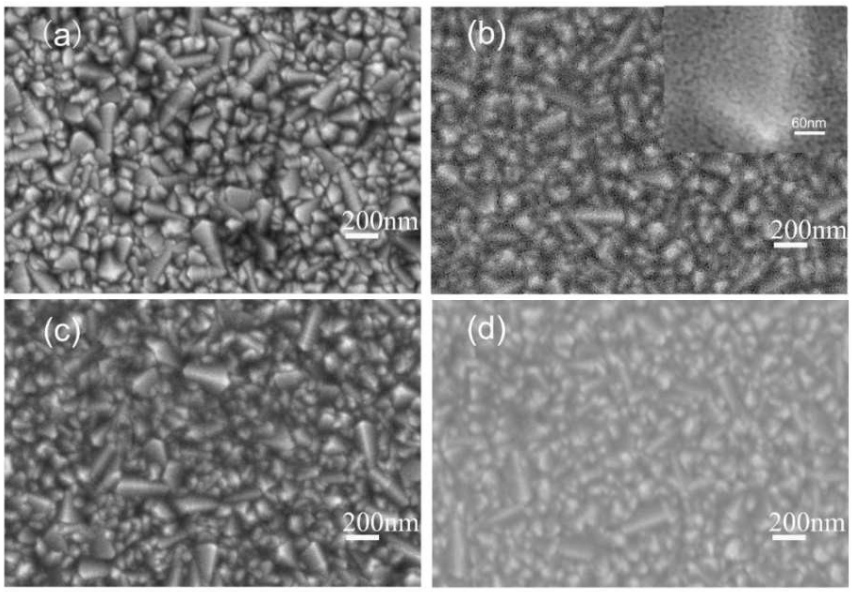

Fig. 3 Top view SEM images of (a) bare FTO; (b) TiO_2 QD compact layer (inset is HRSEM); (c) TAA compact layer; (d) $TiCl_4$ compact layer.

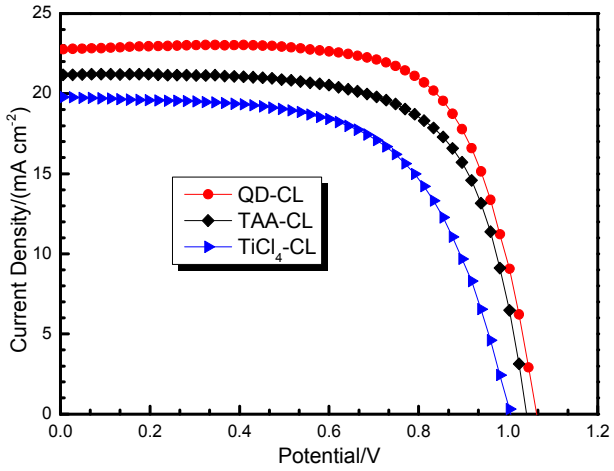

Fig. 4 J-V curves of the perovskite solar cells based on QD-CL, TAA-CL, and $TiCl_4$-CL.

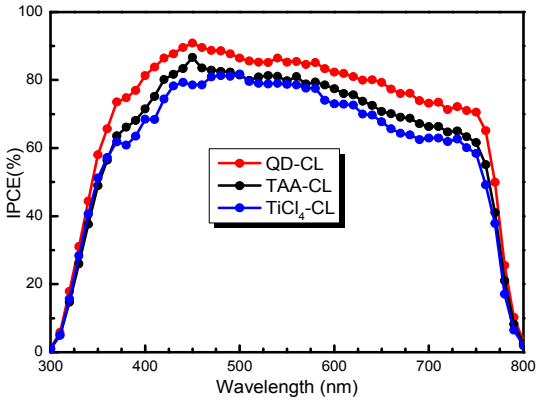

Fig. 5 IPCE spectra of the perovskite solar cells based on QD-CL, TAA-CL, and $TiCl_4$-CL.

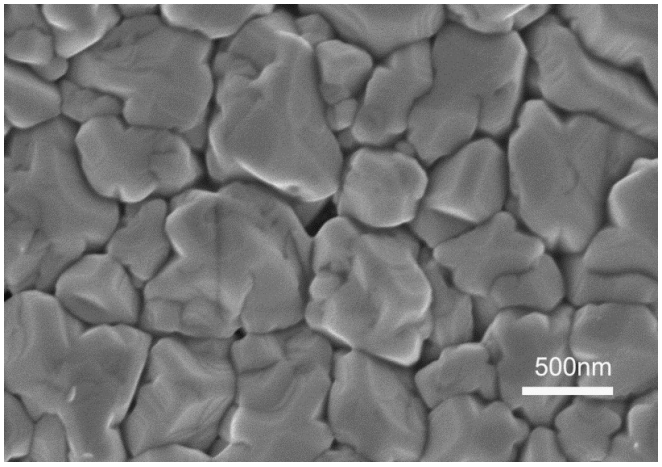

Fig. 6 Top-view SEM image of perovskite $CH_3NH_3PbI_3$ coated on the mesoporous TiO_2 film.

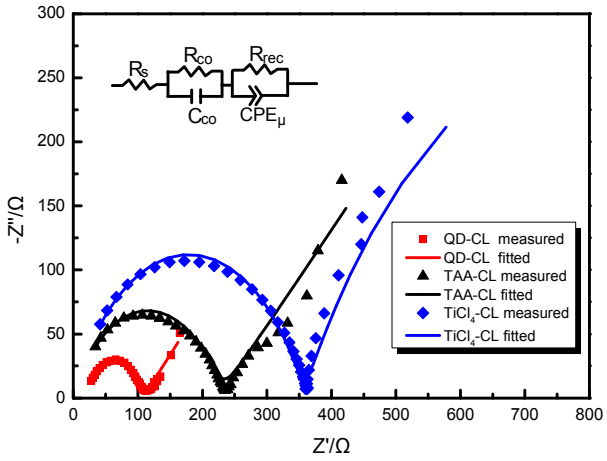

Fig. 7 Nyquist plots of the perovskite solar cells based QD-CL, TAA-CL, $TiCl_4$-CL.

Table 1 Atomic content of TiO_2 QDs

Element	Weight percentage (%)	Atomic percentage (%)
C	5.94	12.47
O	36.25	57.11
Ti	57.81	30.42

Table 2 Photovoltaic performances of the PSCs based on $TiCl_4$-CL with different spin-coating speed and thickness.

Spin-coating speed (rpm)	Thickness(nm)	V_{OC}(V)	J_{SC}(mA·cm^{-2})	FF	PCE(%)
1000	131	0.878	15.41	0.52	7.03
2000	100	0.919	16.75	0.57	8.77
4000	64	0.999	18.49	0.61	11.27
6000	56	0.998	19.03	0.59	11.17

Table 3 Photovoltaic performances of the PSCs based on TAA-CL with different spin-coating speed and thickness.

Spin-coating speed (rpm)	Thickness(nm)	V_{OC}(V)	J_{SC}(mA·cm^{-2})	FF	PCE(%)
1000	90	0.925	17.32	0.66	10.57
2000	72	0.966	18.91	0.64	11.69
4000	58	1.021	19.79	0.67	13.54
6000	44	1.013	20.21	0.65	13.30

Table 4 Photovoltaic performances of the PSCs based on QD-CL with different spin-coating

speed and thickness.

Spin-coating speed (rpm)	Thickness(nm)	V_{OC}(V)	J_{SC}(mA·cm^{-2})	FF	PCE(%)
1000	88	0.959	19.21	0.66	12.16
2000	74	0.979	20.42	0.65	12.99
4000	52	1.049	21.27	0.70	15.62
6000	34	1.038	21.07	0.69	15.09

Table 5 Photovoltaic and resistance parameters of the PSCs with different compact layers.

Compact layers	R_s(Ω cm^2)	R_{sh}(Ω cm^2)	V_{OC}(V)	J_{SC}(mA·cm^{-2})	FF	PCE(%)
QD-CL	5.5	6404	1.063	22.48	0.71	16.97
TAA-CL	8.2	1640	1.041	20.09	0.67	14.01
$TiCl_4$-CL	10.5	955	1.005	19.81	0.63	12.54